Materials Today Sustainability xxx (xxxx) 100261

Contents lists available at ScienceDirect

Materials Today Sustainability

journal homepage: www.elsevier.com

Journal Cover Image

Highly piezoresistive, self-sensing, one-part potassium-activated inorganic polymers for structural health monitoring

M. Di Mare, C.M. Ouellet-Plamondon *

Department of Construction Engineering, École de technologie supérieure, University of Quebec, 1100 Rue Notre-Dame Ouest, Montreal, QC, Canada

ARTICLE INFO

Article history:
Received 27 August 2022
Received in revised form 28 September 2022
Accepted 18 October 2022

Keywords:
Piezoresistivity
Inorganic polymer
Alkali-activated materials
Construction and building materials
Green chemistry

ABSTRACT

Structural health monitoring will revolutionize infrastructure repair by enabling targeted preventative maintenance. To achieve this goal, new self-sensing materials are needed with high strength, piezoresistivity, scalability, and affordability. These four properties can be achieved with potassium-activated inorganic polymers. In this study, new relationships have been discovered between the composition of these materials and their self-sensing capabilities. Alkali-activated materials form natural composites with high self-sensing capabilities without the need for conductive fiber additives. The intrinsic piezoresistivity of potassium-activated inorganic polymers surpasses the best cement-carbon nanotube composites without the added cost and scalability limitations. This positions the materials as the best candidate for future self-sensing construction materials for structural health monitoring applications.

1. Introduction

Structural health monitoring is an emerging technology in construction materials that will fundamentally change the maintenance and repair of concrete buildings. The technology relies on the deployment of self-sensing construction materials in structural members which are capable of reporting changes in their mechanical state. This enables real-time monitoring of structural changes due to corrosion, seismic damage, or structural decay [1]. With improved information, structural health monitoring will make the repair of infrastructure localized and preventive: stopping sites of decay before the impact is systemic [2]. This will substantially reduce the cost of maintenance and prolong the service life of concrete structures and infrastructure. The deployment of structural health monitoring is limited by the availability of self-sensing construction materials. Two principal obstacles that stymie the availability of these materials are high cost and low scalability. These problems arise because Portland cement is not intrinsically self-sensing. It must be combined with conductive additives, preferably fibers such as carbon fiber, to form a self-sensing composite. Cement composites are self-sensing through their piezoresistivity: a measurable reduction in electrical resistance during compression. Carbon fiber-cement composites can achieve piezoresistivity of 10–30% which is suitable for a variety of self-sensing applications [3–5]. However, the reliance on conductive fibers to form self-sensing composites poses multiple problems for the deployment of this technology in the construction sector.

The piezoresistivity of cement composites arises from the tunneling of electrons between the conductive fibers. Cement is an insulating matrix, and the electrical conductivity of cement composites is dominated by the tunneling between the fibers [6]. The tunneling effect is strongly influenced by the distance between the fibers, which is minutely reduced under compressive strain, leading to a macroscopic piezoresistivity. However, because of the extreme sensitivity to the distance fiber spacing, the piezoresistivity of cement composites is highly vulnerable to dispersion irregularities [7,8]. This has led the reported piezoresistivity of cement composites in the literature to vary substantially due to inconsistencies in dispersion methods. In one example, a change in the superplasticizer was reported to increase the piezoresistivity by more than 10× [8]. This presents a problem for the scalability of the technology in the field of construction. Inconsistencies in mixing with different equipment and volumes of production could easily compromise the self-sensing performance.

Proponents of self-sensing cement composites have ambitiously touted these materials as a cost-saving and green solution for the future of construction. Cement production is the singularly largest material contributor to gobal greenhouse gas emissions[9]. Structural health monitoring will prolong the service life of concrete structures thereby reducing maintenance costs and cement consumption. However, few studies have quantified the economic and environmental impact of the

* Corresponding author.
E-mail address: claudiane.ouellet-plamondon@etsmtl.ca (C.M. Ouellet-Plamondon).

https://doi.org/10.1016/j.mtsust.2022.100261
2589-2347/© 20XX

conductive fibers required to produce self-sensing cement composites [10,11]. Many techniques have been investigated to reduce the quantity of conductive fiber required to achieve high piezoresistivity. The most effective method, the use of carbon nanotubes, reduces the required fiber content by at least a factor of 10 [12]. However, the use of nanoparticles amplifies the dispersion sensitivity and the economics of this technique remain uncertain. One study concluded that the use of carbon nanotubes in this manner would increase the cost of cement composites by a factor of 100× compared to ordinary concrete [11].

Additional complications arise from the physical properties of cement composites and the manner of measuring their piezoresistivity. Carbonaceous additives, including carbon fiber and carbon nanotubes, substantially reduce the workability of cement [13–15]. Recent studies have shown that the piezoresistivity of self-sensing cement composites has limited longevity due to breakdown at the fiber-matrix interface [16,17]. Another problem arises from the conventional manner of measuring piezoresistivity. The vast majority of piezoresistivity measurements are conducted under cyclic loading conditions, where the resistance is measured with direct current while the compressive load is oscillated [18]. This method simulates applications involving transient changes in compression, such as vehicle detection on roadways [19]. Cyclic loading, however, is not representative of structural health monitoring applications where gradual changes in static loading indicate corrosion or structural decay. The effectiveness of a self-sensing material for structural health monitoring is better simulated using static loading conditions. However, very few studies have employed static load testing because of the high polarization of cement. Polarization causes the measured electrical resistance under direct current measurements to increase with time which distorts the measurements of the piezoresistivity [20]. Methodologies utilizing alternating currents, such as the one proposed by *Vaidya* et al., remedy this polarization problem but have not seen widespread adoption in the field [21].

The high cost, low scalability, and questionable longevity have stalled the implementation of self-sensing cement composites, and to date, there is no real-world infrastructure that employs this technology [1]. There is a distinct need for an alternative self-sensing material without the problems of cement composites. Very recently, a promising candidate for this role has been found in alkali-activated materials (AAMs). First documented by *Saafi* et al., AAMs exhibit piezoresistivity as an intrinsic material property and, thus, do require need for conductive fibers to act as self-sensing construction materials [22]. Prior studies of AAMs without conductive fibers did not measure any piezoresistivity using direct current [23,24]. However, the work by *Saafi* et al. innovated in its use of an alternating current methodology to avoid the detrimental impact of polarization. With this methodology, AAMs were found to be piezoresistive under static loading conditions, making them ideal self-sensing materials for structural health monitoring applications.

In addition to intrinsic piezoresistivity, AAMs offer numerous advantages over cement as a sustainable structural material. AAMs are natural composites formed from so-called AAM precursors, rich in reactive aluminosilicates. AAMs have been extensively studied as an environmentally friendly cement alternative because several industrial byproducts, such as fly ash and blast furnace slag, can be used as AAM precursors [25]. This causes AAMs to have up to 80% lower global warming potential than Portland cement [26]. Many studies on AAMs have demonstrated a better workability [27,28], higher strength [29,30], and greater durability [31,32] than cement. However, the properties of an AAM are strongly influenced by its chemistry. The chemistry of an AAM is defined by its alkali content, typically described as an alkali/aluminum or alkali/silicon ratio, and its mer structure, defined by the silicon/aluminum ratio. These two compositional parameters determine the number of bridging oxygens and the proportion of siloxo to di-siloxomers within the polymer structure [33].

These compositional factors have a strong impact on the mechanical and electrical properties of AAMs [34,35]. Their relationship to piezoresistivity, an electromechanical property, is entirely unknown. The original work by *Saafi* et al. demonstrated intrinsic piezoresistivity of only a single composition of potassium AAM (K-AAM) [22]. A recent study has corroborated the measurement and test methodology using a sodium AAM, with lower piezoresistivity [36]. However, no investigation has confirmed the intrinsic piezoresistivity of potassium AAMs nor determined the effect of composition on the piezoresistivity of AAMs. This study seeks to address these two research gaps and determine the optimum composition of potassium AAMs to maximize the piezoresistive performance.

2. Materials and methods

2.1. Materials

K-AAMs were prepared by the alkali activation of fly ash. ProAsh® fly ash from Titan America was used and composed of 21.4% aluminum oxide, 55.3% silicon oxide, and 1.0% sodium oxide. An array of AAMs compositions was prepared to achieve potassium/aluminum (K/Al) ratios between 0.8 and 1.2 and silicon/aluminum (Si/Al) ratios between 2.5 and 3.2. The elemental and mixing proportions of the compositions tested are listed in Table 1. The samples were identified with a sequence of two numbers: the K/Al ratio and the Si/Al ratio. Silica fume (4.8% moisture) was added to modulate the Si/Al ratio. Dry reagent grade potassium hydroxide (12% moisture) was the primary activator. For samples C-33, C-67, and C-100, the 33%, 67%, or 100% of the potassium hydroxide was substituted for anhydrous reagent grade potassium carbonate while maintaining the same K/Al ratio. A constant water/binder (W/B) ratio of 0.20 was maintained for all samples to achieve a flowable paste across the range of compositions.

2.2. Mixing and curing procedure

The K-AAMs were mixed in a one-part (single-step) mixing methodology in a planetary cement mixer compliant with ASTM International standard C305 [37]. A one-part methodology based on cement mixing technology was used to maximize the scalability of the process within the current construction industry and circumvent the scalability limitations caused by the two-part mixing of AAMs [38]. The dry powders and water were added simultaneously to the mixer and mixed for 6 min at 45 rpm until a homogenous paste was formed. After mixing, the paste was immediately cast into steel molds coated with petrolatum to

Table 1
Summary of the alkali-activated materials prepared.

Sample ID	K/Al ratio	Si/Al ratio	W/B ratio	Fly ash (g)	Silica fume (g)	Potassium hydroxide (g)	Potassium carbonate (g)	Deionized water (g)
0.8/2.5	0.8	2.50	0.20	500	41.2	92.5	0	113.7
0.8/2.85	0.8	2.85	0.20	500	85.4	92.5	0	120.4
0.8/3.2	0.8	3.20	0.20	500	116.7	92.5	0	127.1
1/2.5	1.0	2.50	0.20	500	41.2	119.2	0	115.8
1/2.85	1.0	2.85	0.20	500	85.4	119.2	0	122.5
1/3.2	1.0	3.20	0.20	500	116.7	119.2	0	129.2
1.2/2.5	1.2	2.50	0.20	500	41.2	145.9	0	117.9
1.2/2.85	1.2	2.85	0.20	500	85.4	145.9	0	124.6
1.2/3.2	1.2	3.20	0.20	500	116.7	145.9	0	131.4
C-33	1.0	2.85	0.20	500	85.4	79.4	43.0	119.6
C-67	1.0	2.85	0.20	500	85.4	39.6	86.2	128.8
C-100	1.0	2.85	0.20	500	85.4	0	129.3	138.0

inhibit adhesion. The molds were sealed in zip-top plastic bags to prevent moisture loss and cured at 60 °C for seven days under saturated humidity conditions to ensure complete hardening. Elevated temperature curing is known to be beneficial for the development of high-strength AAMs and is particularly important for one-part AAMs [38,39].

For mechanical assessment, 50 mm cube specimens were produced in accordance with ASTM C109 [40] and 40 mm × 40 mm × 160 mm square rods were prepared for testing as per ASTM C348 [41]. A sample of each AAM was ground for Fourier transform infrared spectroscopy. For measurement of the piezoresistivity, molds for 50 mm cube specimens were modified with a bracket to hold a pair of electrodes in place during curing. The electrodes were galvanized stainless steel mesh cut to size 50 mm × 100 mm with a wire thickness of 0.61 mm (23 gauge) and mesh size 6.73 mm (mesh #3). The electrodes were embedded 50 mm into the cubes and held parallel at 10 mm apart in the center of one face of the specimen in the manner shown in Fig. 1. Before measurement of the piezoresistivity, the specimen with the embedded electrodes were left to dry in a dry oven at 60 °C for an additional seven days. This drying process gently removed excess surface water from the AAM specimens that could interfere with the resistance measurement through surface conduction without damaging or recrystallizing the native hydrates within the AAMs.

2.3. Characterization methods

The compressive strength was measured in triplicate with a constant loading rate of 1 kN/s, following ASTM C109 [40]. The flexural strength was measured on square rod samples with a constant loading of 0.048 kN/s, as per C348 [41]. Fourier transform infrared spectroscopy was conducted to confirm the complete dissolution of the activator and added silica fume to achieve the targeted elemental proportions in the AAMs. A full spectrum was measured across the range 400 cm^{-1}–4000 cm^{-1}, with special attention paid to 700 cm^{-1}–1300 cm^{-1}, where the characteristic peaks of the alkali activation reaction and recondensation reactions occur.

To measure the piezoresistivity, compressive stress was applied to the AAM specimen with the embedded electrodes at intervals of 1 MPa up to 10 MPa. Compressive stress was applied orthogonal to the orientation of the electrodes, as shown in Fig. 1, such that the distance between the electrodes was reduced by the compressive strain. All measurements were made in triplicate at ambient temperature using samples gently dried using the aforementioned procedure to minimize surface conduction. At each interval of stress, the electrical resistance between the embedded electrodes was measured using a Wheatstone bridge. A Wheatstone bridge is a basic electronic circuit of three resistors used to measure the resistance of an unknown sample under an alternating current. A power source of 10 V was applied at 10 Hz, 10 kHz, and 10 MHz across the bridge, and the sample resistance (R_{sample}) was measured at each frequency using the following equation, derived from Ohms law:

$$R_{sample} = R_3 \frac{R_2 - \frac{V_{measured}}{V_{applied}}\left(R_1 + R_2\right)}{R_1 + \frac{V_{measured}}{V_{applied}}\left(R_1 + R_2\right)}$$

where R_1, R_2, and R_3 are the resistances of the bridge resistors in the orientation shown in Fig. 1, V_{applied} is 10 V, and $V_{measured}$ is the voltage across the sample measured with an oscilloscope. The sample voltage was monitored with an InfiniiVision 3034A oscilloscope from Aligent Technologies®. Resistors of 860 kΩ were used in the Wheatstone bridge to approximate the expected resistance of the AAMs, based on literature values [42], and to maximize the accuracy of the measurement.

Following convention, the piezoresistivity of the AAMs was quantified as the fractional change in resistance (FCR) and its derivatives, the stress sensitivity coefficient, and the gauge factor [18]. The three parameters are defined by the following equations:

$$FCR = \frac{R_\sigma - R_0}{R_0}, \textit{Stress sensitivity}$$
$$= \frac{FCR}{\sigma}, \textit{Gauge factor}$$
$$= \frac{FCR}{\varepsilon}$$

where R_σ is the sample resistance measured at a compressive loading of σ, R_0 is the resistance across the unstressed sample, and ε is the compressive strain. FCR is the clearest representation of the piezoresistivity, but it is dependent on the applied stress. Most commonly, only the maximum FCR measured at the maximum compressive load is discussed. Stress sensitivity and gauge factor serve as comparative tools

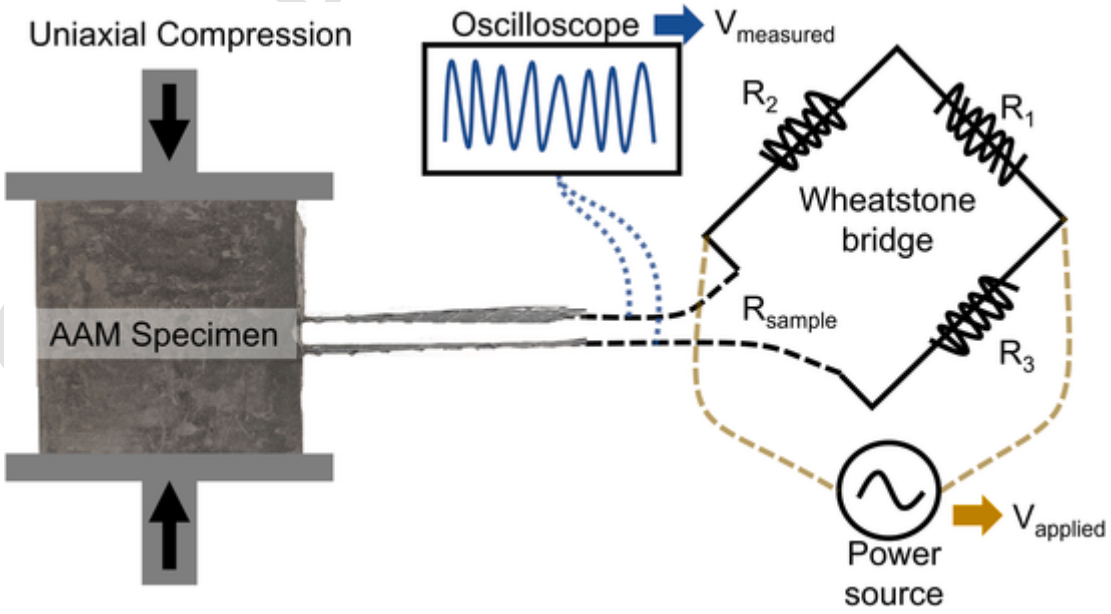

Fig. 1. The experimental set-up for the measurement of the piezoresistivity of the alkali-activated materials using a Wheatstone bridge, oscilloscope, and alternating current power source.

for comparing materials tested under different levels of compressive loading.

3. Results and discussion

3.1. The intrinsic piezoresistivity of AAMs

The intrinsic piezoresistivity of AAMs is an opportunity to make affordable and environmentally friendly self-sensing construction materials from industrial byproducts. AAMs are a cost-competitive alternative to ordinary Portland cement and their production from industrial byproducts, such as the fly ash utilized in this study, offer a substantially reduced carbon footprint for a construction material. The discovery of their self-sensing functionality presents an added advantage which could see the rapid incorporation of smart construction materials in all forms of construction. This is possible because their self-sensing behavior is intrinsic and is achieved without the added cost of additives or the exotic coating methods required by conventional self-sensing technology [43]. However, the intrinsic piezoresistivity in AAMs is a recent discovery and the field is not yet aware of the remarkable potential.

The piezoresistivity of AAMs has escaped scientific scrutiny thus far because its detection requires a non-standard measurement method. AAMs have been previously studied as an alternative binder to cement for self-sensing composites with carbon fiber and other conductive additives [44]. Nearly every study in the literature has omitted reporting the piezoresistivity of neat AAMs, AAMs without any additive, as a baseline. This is presumably because the high dielectric polarization of neat AAMs makes the measurement of the electrical resistance highly inconsistent under direct current conditions [42]. This has led to the erroneous conclusion that AAMs are not intrinsically piezoresistive [44]. However, this hypothesis was disproven by the recent publication by *Saafi* et al. that measures the piezoresistivity using alternating current [22]. Without the obscuration of polarization, AAMs exhibit relatively high piezoresistivity as an intrinsic property.

Competing theories exist on the nature of the intrinsic piezoresistivity in AAMs. The property has been likened to the piezoelectricity of AAMs, another electromechanical property, which is caused by the high mobility of alkali cations within the amorphous structure [22,45,46]. The alkali cations, typically sodium or potassium depending on the alkali activator, charge balance the aluminosilicate polymer network in AAMs and are free to migrate between adjacent sites [33]. A recent publication, corroborating the results of *Saafi* et al., alternatively proposed that the piezoresistivity is not dominated by the ionic movement but instead by changes in the electronic mobility [36]. However, these two works disagree on the magnitude of the measured piezoresistivity. The works did not use the same composition, and it is well known that the properties of an AAM are strongly influenced by its composition. No study has yet determined what factor or combination of factors controls the piezoresistivity of AAMs.

The most significant difference between the AAMs in the two prior publications is their alkali activator. *Saafi* et al. tested potassium-activated fly ash (K-AAMs) while the other used the more common sodium-activated fly ash (Na-AAMs) [22,36]. Na-AAMs and K-AAMs are typically modeled as modified Nepheline and Leucite crystals, visualized in Fig. 2(a). The different size of the activator cation has a substantial impact on the symmetry of the crystal structure and its geometry. To quantify the role of activator cation in the piezoresistivity, two compositions of AAMs were prepared with identical alkali/aluminum (alkali/Al) and silicon aluminum (Si/Al) ratios using sodium hydroxide and potassium hydroxide as activators. The piezoresistivity of the samples was measured as the samples were compressed at intervals up to 10 MPa and the results are presented in Fig. 2(b–d). Both specimens exhibited acceptable compressive strength, above 30 MPa, and high piezoresistivity. With these properties, both AAMs would make suitable materials for structural health monitoring applications.

The K-AAMs in Fig. 2(c) had a significantly greater piezoresistive response than the Na-AAMs equivalent. The K-AAMs reached a FCR > 60%. This is a substantial improvement over typical cement composites, which generally yield 10–30% FCR, similar to the Na-AAMs measured here [47]. While the Na-AAM is a good self-sensing material, the result confirms that the piezoresistivity is strongly influenced by the activator cation. It agrees with the prior two studies that potassium is a preferred activator for self-sensing AAMs, giving higher FCR. The FCR was also found to decline following an exponential curve at higher frequencies, as has been previously reported [36]. However,

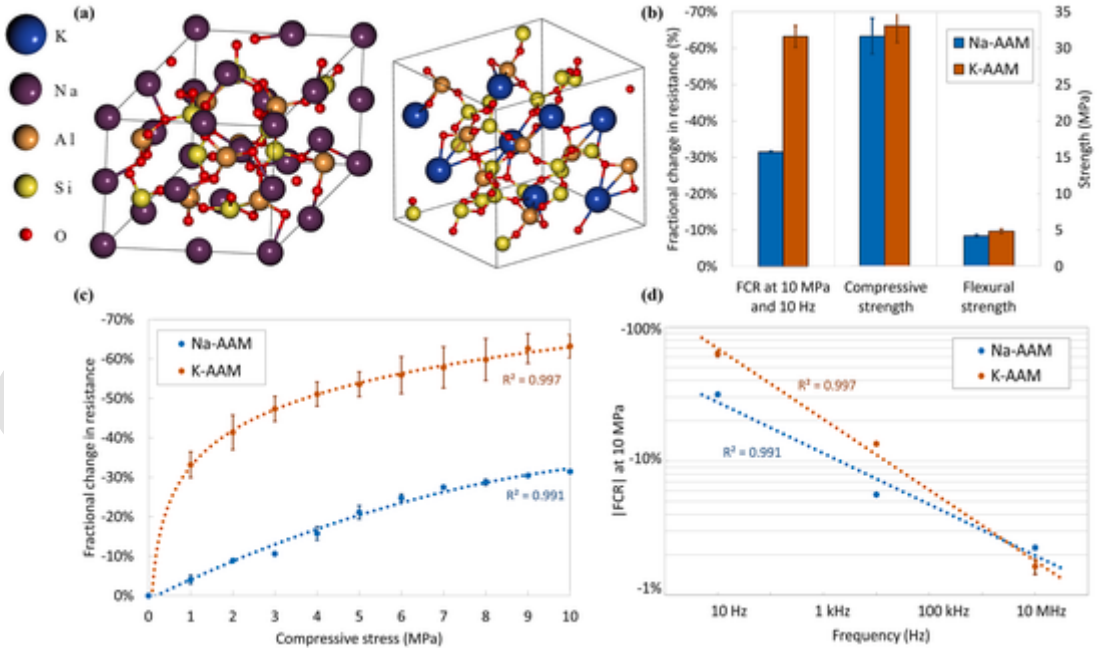

Fig. 2. (**a**) Visualizations of the Nepheline and Leucite crystal structures. (**b**) A comparison of the piezoresistivity and mechanical properties of the sodium and potassium alkali-activated materials. (**c**), (**d**) The fractional change in resistance of sodium (Na-AAMs) and potassium (K-AAMs) alkali-activated materials with alkali/Al ratio of 1.0 and Si/Al ratio of 2.85.

the magnitude of the FCR measured for this K-AAM was dramatically higher than that measured by *Saafi* et al. in their work, which was 16–22% at the same frequency and compression [22]. This indicates that the additional compositional factors are involved in controlling the piezoresistivity of K-AAMs.

3.2. Compositional optimization to maximize the piezoresistivity of AAMs

The alkali content (K/Al) and chain structure (Si/Al) strongly impact the physical, mechanical, and electrical properties of AAMs [34,35]. To investigate the impact of these compositional factors on the piezoresistivity, an array of compositions was prepared to expand around the initial K-AAM composition in a full factorial design. The piezoresistivity measurements at each frequency are presented in Table 2. As with the initial Na-AAM and K-AAM compositions, the piezoresistivity of the AAMs declines following a power function with frequency. The FCR was reduced below 20% at 10 kHz and became negligible in the MHz range. This trend was consistent for all of the compositions and not influenced by any of the compositional factors. At 10 Hz, exceptionally high FCR was measured for all the compositions. All the compositions were above 45% and the highest reached 67% FCR.

Table 2
The electrical resistance and piezoresistivity of an array of potassium-activated materials.

Sample ID	Resistance under0 MPa load (MΩ)[a]	Resistance under 10 MPa load (MΩ)[a]	Fractional change in resistance under 10 MPa load (%)		
			at 10 Hz	at 10 kHz	at 10 MHz
0.8/2.5	0.615	0.316	48.8	9.5	0.2
0.8/2.85	0.766	0.269	67.0	17.0	0.7
0.8/3.2	0.794	0.431	54.1	14.2	0.5
1/2.5	0.703	0.290	58.2	11.9	0.5
1/2.85	0.786	0.323	61.1	11.9	1.0
1/3.2	0.843	0.391	53.5	11.0	0.8
1.2/2.5	0.694	0.340	48.7	10.5	0.3
1.2/2.85	0.617	0.293	57.4	17.7	0.1
1.2/3.2	0.616	0.286	50.9	17.1	0.1

[a] Electrical resistance measured with a testing frequency of 10 Hz between electrodes 10 mm apart.

Interpreting these results involves deconvolving the composition into its constituent elemental ratios. AAMs across the compositional range followed similar FCR trends with applied stress, shown in Fig. 3 (a). The piezoresistivity shows some nonlinearity at low stress but becomes linear at higher levels of compression. This trend, like the frequency dependence, was not influenced by the composition. The FCR measured under a compressive load of10 MPa, showed strong dependence on both compositional factors. The FCR was improved by varying the Si/Al ratio, and an optimum was found at the midpoint of the array, 2.85. The Si/Al ratio governs the chain structure of the AAMs. When the Si/Al ratio is between 2 and 3, the AAM is composed of a mixture of siloxo and di-siloxo mers. Above 3.0, the AAM is saturated with silica, and the excess forms crosslinking silate groups between the polymer chains [33]. The results, shown in Fig. 3(c), reveal that the piezoresistivity is maximized when the Si/Al ratio is between 2.7 and 3.0, with the FCR declining parabolically away from the optimum. This indicates that a minority of siloxo mers distributed in a matrix of predominately di-siloxo mers is preferable for developing a chain structure with strain-sensitive conductivity. An absence of siloxo mers or an excess of di-siloxo mers reduces the piezoresistive response. The optimum Si/Al ratio appears to be influenced by the K/Al ratio, which also strongly impacts the piezoresistivity.

The K/Al ratio has a more complicated relationship with the piezoresistivity, as shown in Fig. 3(d). Potassium ions in an AAM act as

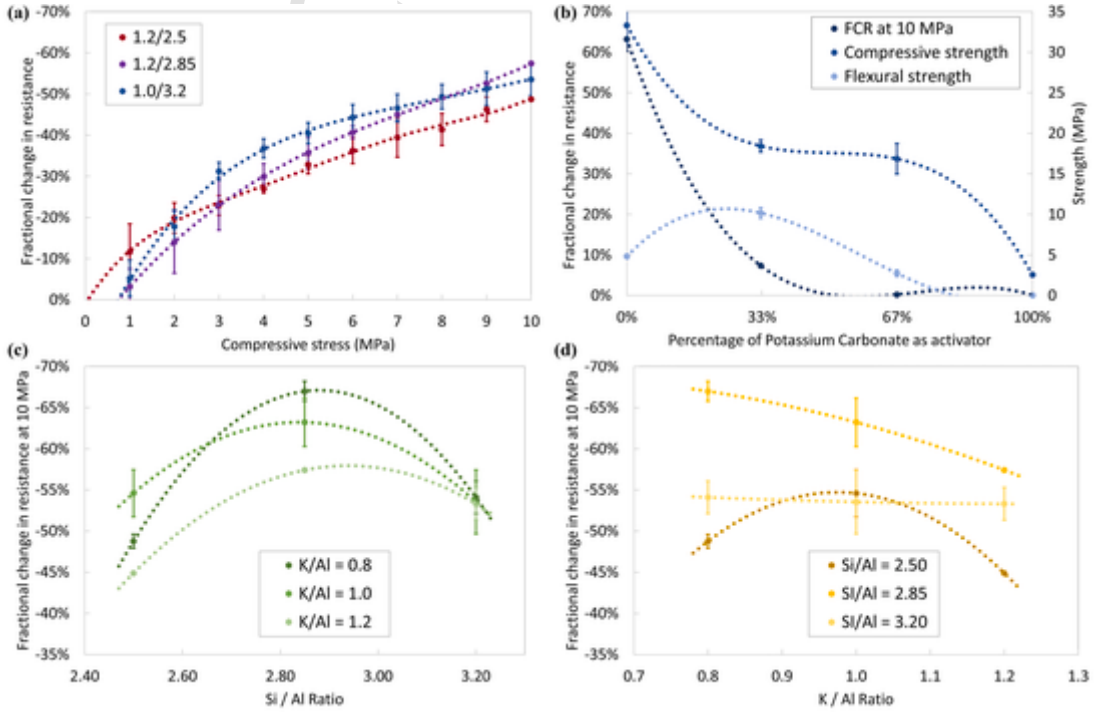

Fig. 3. (**a**) The fractional change in resistance with compressive stress for AAMs with different compositions. (**b**) The effect of potassium carbonate as an alternative activator on the piezoresistivity and the strength of the AAMs. A comparison of the piezoresistivity under a compressive load of 10 MPa and with an alternating current source at 10 Hz for AAMs with different (**c**) K/Al ratios and (**d**) Si/Al ratios.

charge balancing species, localized around alumina tetrahedra. When the K/Al ratio is above 1.0, there is a supersaturation of potassium ions. Contrary to expectations, this does not improve the piezoresistive response despite improving the conductivity, as listed in Table 2. Instead, the piezoresistivity declines above 1.0, indicating that these extra-stoichiometric potassium ions are mobile but not sensitive to strain. For K/Al below 1.0, the presence of potassium vacancies increases the number of bridging oxygens to compensate for the charge imbalance. When there are more siloxo mers in the chain structure, an increase in bridging oxygens causes a reduction in the piezoresistivity. However, near the optimum Si/Al ratio the trend is reversed. A K/Al ratio below parity significantly improves the FCR up to 67%, suggesting that bridging oxygens play a critical role in the strain-sensitive conduction pathways that cause the piezoresistivity. This gives insight into the mechanisms of the intrinsic piezoresistivity in AAMs though the computational modeling of AAMs is limited and a more thorough investigation of this topic is required for a deeper analysis of the piezoresistive mechanisms [36].

The K/Al and Si/Al are not independent factors in controlling the piezoresistivity of the AAMs. Both factors significantly influence the piezoresistivity and their interdependence must be considered in the design of self-sensing AAMs. To visualize the relationship, the results over the full array of compositions are presented in a 3-dimensional rendering and 2-dimensional contour plot in Fig. 4. In this figure, the lowest valley, shown in red, gives the greatest FCR and thus the best piezoresistivity. While there is some apparent symmetry in the topography, the relationship, even in this relatively small compositional range, is complex and dependent on both factors. This visualization allows for the facile identification of the most desirable compositional ranges to investigate for self-sensing AAMs. On the surface, it may seem that further reduction in the K/Al would be preferable for self-sensing applica-

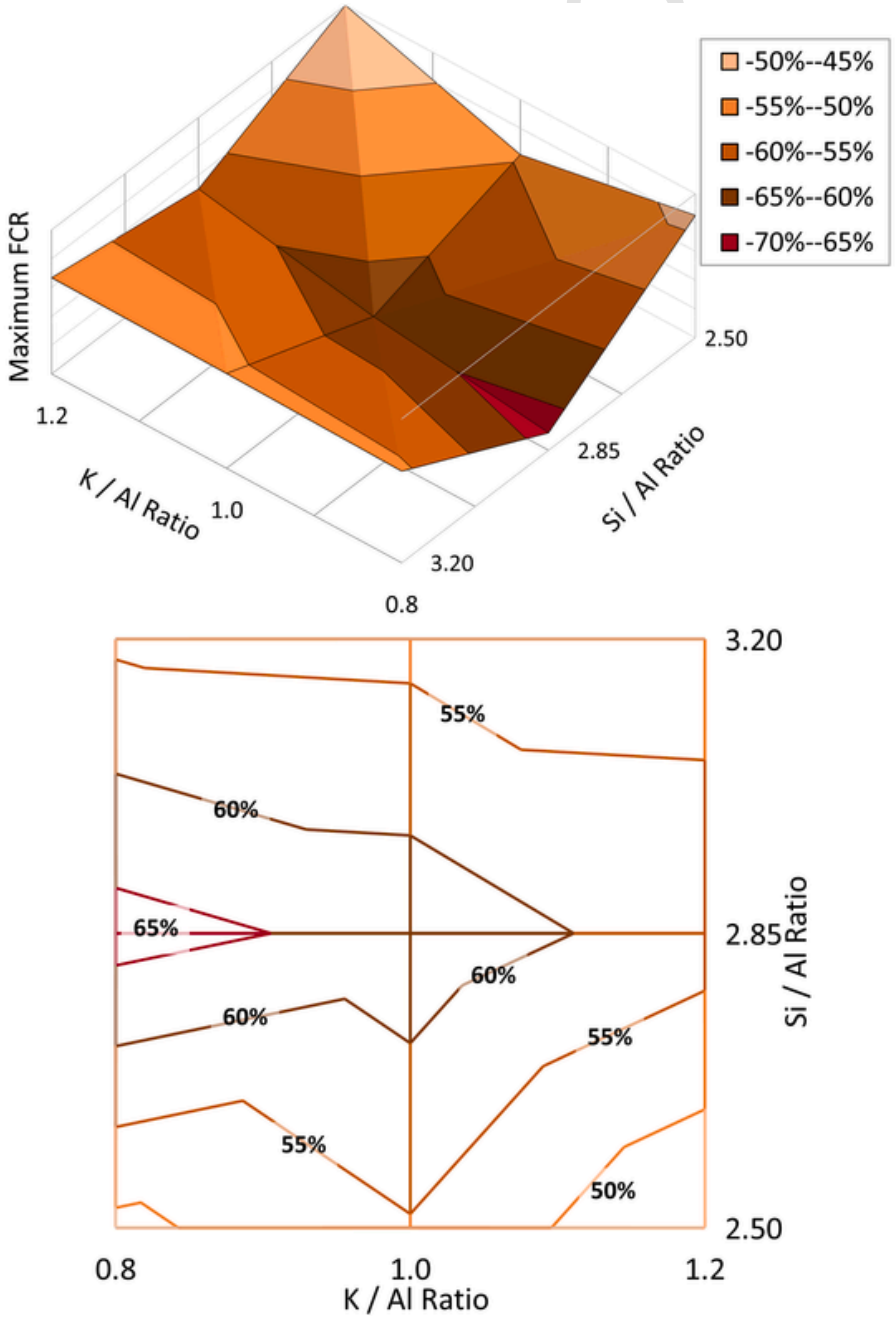

Fig. 4. The compositional dependence of the piezoresistivity of alkali-activated materials measured under a compressive load of 10 MPa and with an alternating current source of 10 Hz, shown as a 3D rendering and a 2D contour plot.

tions. However, there are trade-offs with the mechanical properties, discussed in Section 3.3, which make this avenue impractical.

Another compositional factor that can influence the mechanical properties is the activator anion. The activator in a K-AAM is a salt of potassium and the anion in the activator can influence the mechanical properties, setting rate, and environmental impact of an AAM [48]. A recent study of K-AAMs revealed that the electrical properties are strongly influenced by the activator anion. In that study, the conductivity was improved by several orders of magnitude by replacing the potassium hydroxide activator with potassium carbonate [42]. To probe the effect of the activator anion on the piezoresistivity, a series of AAMs were prepared to partially substitute the primary activator, potassium hydroxide, for potassium carbonate between 33% and 100%, while maintaining the same elemental composition. The results, presented in Fig. 3(b), show that the piezoresistivity and compressive strength decline sharply when potassium carbonate is used as the activator. The AAM, which gave a very high performance with potassium hydroxide, loses all of its piezoresistivity when 67% and 100% of the activator is potassium carbonate. This is caused by the substantially higher conductivity of the potassium carbonate AAMs achieving an effect similar to the percolation threshold in conventional cement composites [6]. The network of conductivity becomes continuous for potassium carbonate AAMs, and resistance becomes no longer susceptible to strain. Thus, the piezoresistivity vanishes. This observation indicates the importance of the activator anion and other factors known to influence the conductivity when optimizing self-sensing AAMs.

3.3. The outlook for self-sensing AAMs for structural health monitoring

Self-sensing construction materials must achieve high piezoresistivity and high mechanical strength. However, a quantified definition of "high piezoresistivity" is yet to be defined. Self-sensing construction materials are in their infancy and they have not yet been tested in real-world infrastructure projects [1]. As such, no criterion has been established for the level of FCR required for structural health monitoring applications. Materials with higher FCR should have significantly improved sensitivity to detect changes in compressive loading. In principle, this reduces the threshold for the early detection of corrosion or damage. Thus, maximizing the FCR improves the self-sensing performance, and no upper limit has been identified. In contrast, mechanical requirements are well established and vary based on the application. For load-bearing structural members, an ultimate compressive strength of 28 MPa is required [40]. However, the requirements are lower for other applications such as bricks (20.7 MPa) and non-load-bearing members (4.1 MPa) [49,50]. For self-sensing materials, maximizing the FCR must be balanced by maintaining the required mechanical properties for construction applications.

The mechanical and piezoresistive properties of the three compositions of K-AAMs with the highest FCR are listed in Table 3. These AAMs share the optimum Si/Al ratio which was shown to give the highest piezoresistive performance. Though the composition '0.8/2.85' exhibited the greatest FCR, the compressive strength decreased dramatically at lower K/Al. This trend is consistent with other studies of the effect of the alkali/aluminum ratio on compressive strength [34]. The composition '1/2.85' has a superior combination of properties because it achieves high piezoresistivity and sufficient strength to be used in load-bearing members.

Table 3
The piezoresistivity and mechanical properties of the optimal compositions of alkali-activated materials.

Sample ID	Compressive strength (MPa)	Flexural strength (MPa)	Fractional change in resistance[a] (%)	Stress sensitivity (MPa^{-1})	Gauge factor
0.8/2.85	12.9	3.3	67.0	0.067	39.3
1.0/2.85	33.3	4.8	63.2	0.063	95.7
1.2/2.85	20.5	3.9	57.4	0.057	53.5

[a] Measured under a compressive load of 10 MPa with a 10 Hz alternating current source.

The intrinsic piezoresistivity of K-AAMs creates a unique opportunity to create a superior self-sensing construction material without the drawbacks of conventional composites. With compositional optimization, the piezoresistivity can be more than tripled compared to the original study by *Saafi* et al. [22]. The K-AAMs developed in this study outperformed nearly every AAM composite containing carbon fiber, carbon nanotubes, or graphene in the literature. Many studies dispersing carbonaceous additives in AAMs have reported only roughly 5% FCR [51,52]. However, studies with greater dispersion and high concentrations of fibers have reached FCR of 15–30% [21,23,53]. These results are on par with cement composites that have reported FCR between 10 and 30% using various dosages and combinations of conductive additives [3,5,12,54]. Though there are some examples in the literature of piezoresistive composites with FCR comparable to that of K-AAMs, 40–70%, the methods required to prepare these composites involve extreme dispersion-assistance or exotic-coating methods to achieve this property [8,55]. Intrinsically piezoresistive K-AAMs offer a distinct advantage in the simplicity of their production.

Structural health monitoring technology is stagnant because self-sensing construction materials have not yet been able to make the transition from laboratory development to scalable production. This is a consequence of the distinct challenge in scaling the technology used to make conventional self-sensing composites. Even small quantities of highly refined conductive fibers can dramatically inflate the cost of the composites and the sustainability of cement composites has not received scientific attention [10,11]. Moreover, the composites have questionable longevity and reproducibility which is an unacceptable tradeoff in load-bearing structures where consistency and long-term performance are of paramount importance [16,17]. The construction industry is ill-equipped to utilize the high-energy dispersion techniques required to achieve consistent properties in these composites and this creates a tremendous obstacle to the widespread adoption of these technologies [2,18]. Intrinsically piezoresistive K-AAMs are a much-needed alternative to cement composites. They can be prepared in a standard cement mixer in a single-step process without exotic additives, maximizing their scalability in the construction sector. Their piezoresistivity dwarfs conventional composites without the added cost, complexity, and environmental impact of added carbon fiber. This makes K-AAMs the most promising self-sensing material for the smarter and greener construction of the future.

4. Conclusion

AAMs are an alternative self-sensing material that will revolutionize the field of smart construction materials. Conventional self-sensing composites are limited in scalability because of the conductive additives required. AAMs dramatically improve on this approach by achieving high piezoresistivity intrinsically, without the need for any additives. This presents a far greener, more scalable, and more affordable alternative to conventional composites without sacrificing mechanical integrity. The self-sensing capability of AAMs has not received scientific attention previously because of the sensitivity of this property to composition. More investigations are needed on the measurement set-up, material composition, and the benchmark to other materials. This study presents a compositional optimization for potassium AAMs based on fly ash using a one-part (single-step) mixing process in a standard cement mixer. This makes AAMs a drop-in replacement for construction materials while adding smart functionality to enable structural health monitoring and improve sustainability.

Author contributions

Michael Di Mare: Conceptualization, Methodology, Investigation, Formal analysis, Writing – Original Draft, Writing – Review & Editing, Visualization.

Claudiane Ouellet-Plamondon: Conceptualization, Supervision, Project administration, Funding acquisition, Writing – Review & Editing.

Declaration of competing interest

The authors declare that they have no known competing financial interests or personal relationships that could have appeared to influence the work reported in this paper.

Data availability

Data will be made available on request.

Acknowledgment

The authors would like to thank the Natural Sciences and Engineering Research Council of Canada for their support of this research.

References

[1] Z. Tian, Y. Li, J. Zheng, S. Wang, A state-of-the-art on self-sensing concrete: materials, fabrication and properties, Compos. B Eng. 177 (2019) 107437, https://doi.org/10.1016/j.compositesb.2019.107437.
[2] P.N. Reddy, B.V. Kavyateja, B.B. Jindal, Structural health monitoring methods, dispersion of fibers, micro and macro structural properties, sensing, and mechanical properties of self-sensing concrete—a review, Struct. Concr. 22 (2021) 793–805, https://doi.org/10.1002/suco.202000337.
[3] F. Azhari, N. Banthia, Cement-based sensors with carbon fibers and carbon nanotubes for piezoresistive sensing, Cement Concr. Compos. 34 (2012) 866–873.
[4] M. Chen, P. Gao, F. Geng, L. Zhang, H. Liu, Mechanical and smart properties of carbon fiber and graphite conductive concrete for internal damage monitoring of structure, Construct. Build. Mater. 142 (2017) 320–327.
[5] J. Donnini, T. Bellezze, V. Corinaldesi, Mechanical, electrical and self-sensing properties of cementitious mortars containing short carbon fibers, J. Build. Eng. 20 (2018) 8–14, https://doi.org/10.1016/j.jobe.2018.06.011.
[6] E. García-Macías, R. Castro-Triguero, A. Sáez, F. Ubertini, 3D mixed micromechanics-FEM modeling of piezoresistive carbon nanotube smart concrete, Comput. Methods Appl. Mech. Eng. 340 (2018) 396–423.
[7] O. Galao, F.J. Baeza, E. Zornoza, P. Garcés, Strain and damage sensing properties on multifunctional cement composites with CNF admixture, Cement Concr. Compos. 46 (2014) 90–98, https://doi.org/10.1016/j.cemconcomp.2013.11.009.
[8] B. Han, K. Zhang, X. Yu, E. Kwon, J. Ou, Fabrication of piezoresistive CNT/CNF cementitious composites with superplasticizer as dispersant, J. Mater. Civ. Eng. 24 (2012) 658–665, https://doi.org/10.1061/(ASCE)MT.1943-5533.0000435.
[9] R.M. Andrew, Global CO 2 emissions from cement production, Earth Syst. Sci. Data 10 (2018) 195–217.
[10] I. Papanikolaou, N. Arena, A. Al-Tabbaa, Graphene nanoplatelet reinforced concrete for self-sensing structures – a lifecycle assessment perspective, J. Clean. Prod. 240 (2019) 118202, https://doi.org/10.1016/j.jclepro.2019.118202.
[11] S. Gupta, J.G. Gonzalez, K.J. Loh, Self-sensing concrete enabled by nano-engineered cement-aggregate interfaces, Struct. Health Monit. 16 (2017) 309–323, https://doi.org/10.1177/1475921716643867.
[12] D.-Y. Yoo, S. Kim, S.H. Lee, Self-sensing capability of ultra-high-performance concrete containing steel fibers and carbon nanotubes under tension, Sens. Actuators A: Physical. 276 (2018) 125–136.
[13] C. Bhojaraju, S.S. Mousavi, V. Brial, M. DiMare, C.M. Ouellet-Plamondon, Fresh and hardened properties of GGBS-contained cementitious composites using graphene and graphene oxide, Construct. Build. Mater. 300 (2021) 123902, https://doi.org/10.1016/j.conbuildmat.2021.123902.
[14] H. Wang, X. Gao, R. Wang, The influence of rheological parameters of cement paste on the dispersion of carbon nanofibers and self-sensing performance, Construct. Build. Mater. 134 (2017) 673–683, https://doi.org/10.1016/j.conbuildmat.2016.12.176.
[15] P.F.G. Banfill, G. Starrs, G. Derruau, W.J. McCarter, T.M. Chrisp, Rheology of low carbon fibre content reinforced cement mortar, Cement Concr. Compos. 28 (2006) 773–780, https://doi.org/10.1016/j.cemconcomp.2006.06.004.
[16] H. Wang, X. Gao, J. Liu, Effects of salt freeze-thaw cycles and cyclic loading on the piezoresistive properties of carbon nanofibers mortar, Construct. Build. Mater. 177 (2018) 192–201, https://doi.org/10.1016/j.conbuildmat.2018.05.103.
[17] H. Li, H. Xiao, J. Ou, Electrical property of cement-based composites filled with carbon black under long-term wet and loading condition, Compos. Sci. Technol. 68 (2008) 2114–2119, https://doi.org/10.1016/j.compscitech.2008.03.007.
[18] B. Han, S. Ding, X. Yu, Intrinsic self-sensing concrete and structures: a review, Measurement 59 (2015) 110–128, https://doi.org/10.1016/j.measurement.2014.09.048.
[19] B. Han, X. Yu, E. Kwon, A self-sensing carbon nanotube/cement composite for traffic monitoring, Nanotechnology 20 (2009) 445501, https://doi.org/10.1088/0957-4484/20/44/445501.
[20] X. Fu, E. Ma, D.D.L. Chung, W.A. Anderson, Self-monitoring in carbon fiber reinforced mortar by reactance measurement, Cement Concr. Res. 27 (1997) 845–852, https://doi.org/10.1016/S0008-8846(97)83277-2.
[21] S. Vaidya, E. Allouche, Experimental evaluation of electrical conductivity of carbon fiber reinforced fly-ash based geopolymer, Smart Struct. Syst. 7 (2011) 27–40.
[22] M. Saafi, A. Gullane, B. Huang, H. Sadeghi, J. Ye, F. Sadeghi, Inherently multifunctional geopolymeric cementitious composite as electrical energy storage and self-sensing structural material, Compos. Struct. 201 (2018) 766–778, https://doi.org/10.1016/j.compstruct.2018.06.101.
[23] L. Deng, Y. Ma, J. Hu, S. Yin, X. Ouyang, J. Fu, A. Liu, Z. Zhang, Preparation and piezoresistive properties of carbon fiber-reinforced alkali-activated fly ash/slag mortar, Construct. Build. Mater. 222 (2019) 738–749, https://doi.org/10.1016/j.conbuildmat.2019.06.134.
[24] C. Mizerová, I. Kusák, L. Topolář, P. Schmid, P. Rovnaník, Self-sensing properties of fly ash geopolymer doped with carbon black under compression, Materials 14 (2021) 4350, https://doi.org/10.3390/ma14164350.
[25] P. Duxson, J.L. Provis, Designing precursors for geopolymer cements, J. Am. Ceram. Soc. 91 (2008) 3864–3869, https://doi.org/10.1111/j.1551-2916.2008.02787.x.
[26] G. Habert, C.M. Ouellet-Plamondon, Recent Update on the Environmental Impact of Geopolymers, RILEM Tech. Lett. 1 (2016) 17–23, https://doi.org/10.21809/rilemtechlett.2016.6.
[27] J.G. Jang, N. Lee, H.-K. Lee, Fresh and hardened properties of alkali-activated fly ash/slag pastes with superplasticizers, Construct. Build. Mater. 50 (2014) 169–176.
[28] M. Alonso, S. Gismera, M. Blanco, M. Lanzón, F. Puertas, Alkali-activated mortars: workability and rheological behaviour, Construct. Build. Mater. 145 (2017) 576–587.
[29] W.K. Part, M. Ramli, C.B. Cheah, An overview on the influence of various factors on the properties of geopolymer concrete derived from industrial by-products, Construct. Build. Mater. 77 (2015) 370–395, https://doi.org/10.1016/j.conbuildmat.2014.12.065.
[30] Y. Ding, J.-G. Dai, C.-J. Shi, Mechanical properties of alkali-activated concrete: a state-of-the-art review, Construct. Build. Mater. 127 (2016) 68–79, https://doi.org/10.1016/j.conbuildmat.2016.09.121.
[31] S.A. Bernal, J.L. Provis, Durability of alkali-activated materials: progress and perspectives, J. Am. Ceram. Soc. 97 (2014) 997–1008.
[32] J. Zhang, C. Shi, Z. Zhang, Z. Ou, Durability of alkali-activated materials in aggressive environments: a review on recent studies, Construct. Build. Mater. 152 (2017) 598–613, https://doi.org/10.1016/j.conbuildmat.2017.07.027.
[33] J. Davidovits, Geopolymers, J. Therm. Anal. Calorim. 37 (1991) 1633–1656, https://doi.org/10.1007/BF01912193.
[34] M. Rowles, B. O'connor, Chemical optimisation of the compressive strength of aluminosilicate geopolymers synthesised by sodium silicate activation of metakaolinite, J. Mater. Chem. 13 (2003) 1161–1165.
[35] S. Hanjitsuwan, S. Hunpratub, P. Thongbai, S. Maensiri, V. Sata, P. Chindaprasirt, Effects of NaOH concentrations on physical and electrical properties of high calcium fly ash geopolymer paste, Cement Concr. Compos. 45 (2014) 9–14, https://doi.org/10.1016/j.cemconcomp.2013.09.012.
[36] M. Di Mare, N. Inumerable, P.P. Brisebois, C.M. Ouellet-Plamondon, Combined experimental and computational prediction of the piezoresistivity of alkali-activated inorganic polymers, J. Phys. Chem. C (2022), https://doi.org/10.1021/acs.jpcc.2c03633.
[37] ASTM International, ASTM C305-12 Practice for Mechanical Mixing of Hydraulic Cement Pastes and Mortars of Plastic Consistency, 2020, https://doi.org/10.1520/C0305-12.
[38] T. Luukkonen, Z. Abdollahnejad, J. Yliniemi, P. Kinnunen, M. Illikainen, One-part alkali-activated materials: a review, Cement Concr. Res. 103 (2018) 21–34, https://doi.org/10.1016/j.cemconres.2017.10.001.
[39] T. Suwan, M. Fan, Effect of manufacturing process on the mechanisms and mechanical properties of fly ash-based geopolymer in ambient curing temperature, Mater. Manuf. Process. 32 (2017) 461–467.
[40] ASTM International, ASTM C109/C109M-20B Test Method for Compressive Strength of Hydraulic Cement Mortars (Using 2-in. or [50-mm] Cube Specimens), 2020, https://doi.org/10.1520/C0109_C0109M-20B.
[41] ASTM International, ASTM C348-21 Test Method for Flexural Strength of Hydraulic-Cement Mortars, 2021, https://doi.org/10.1520/C0348-21.
[42] M. Di Mare, C. Ouellet-Plamondon, The effect of composition on the dielectric properties of alkali activated materials: a next generation dielectric ceramic, Mater. Today Commun. 32 (2022) 104087, https://doi.org/10.1016/j.mtcomm.2022.104087.
[43] W. Li, W. Dong, Y. Guo, K. Wang, S.P. Shah, Advances in multifunctional cementitious composites with conductive carbon nanomaterials for smart infrastructure, Cement Concr. Compos. 128 (2022) 104454, https://doi.org/10.1016/j.cemconcomp.2022.104454.
[44] Z. Tang, W. Li, Y. Hu, J.L. Zhou, V.W.Y. Tam, Review on designs and properties of multifunctional alkali-activated materials (AAMs), Construct. Build. Mater. 200 (2019) 474–489, https://doi.org/10.1016/j.conbuildmat.2018.12.157.
[45] C. Lamuta, S. Candamano, F. Crea, L. Pagnotta, Direct piezoelectric effect in geopolymeric mortars, Mater. Des. 107 (2016) 57–64.

[46] C. Lamuta, L. Bruno, S. Candamano, L. Pagnotta, Piezoresistive characterization of graphene/metakaolin based geopolymeric mortar composites, MRS Adv. 2 (2017) 3773–3779, https://doi.org/10.1557/adv.2017.595.
[47] W. Li, F. Qu, W. Dong, G. Mishra, S.P. Shah, A comprehensive review on self-sensing graphene/cementitious composites: a pathway toward next-generation smart concrete, Construct. Build. Mater. 331 (2022) 127284, https://doi.org/10.1016/j.conbuildmat.2022.127284.
[48] S.A. Bernal, Advances in near-neutral salts activation of blast furnace slags, RILEM Tech. Lett. 1 (2016) 39–44, https://doi.org/10.21809/rilemtechlett.2016.8.
[49] ASTM International, ASTM C62-17 Standard Specification for Building Brick (Solid Masonry Units Made from Clay or Shale), 2017. https://www.astm.org/c0062-17.html.
[50] ASTM International, ASTM C129-17 Standard Specification for Nonloadbearing Concrete Masonry Units, 2022. https://www.astm.org/c0129-17.html.
[51] J.L. Vilaplana, F.J. Baeza, O. Galao, E. Zornoza, P. Garcés, Self-sensing properties of alkali activated blast furnace slag (BFS) composites reinforced with carbon fibers, Materials 6 (2013) 4776–4786, https://doi.org/10.3390/ma6104776.
[52] M. Perry, M. Saafi, G. Fusiek, P. Niewczas, Hybrid optical-fibre/geopolymer sensors for structural health monitoring of concrete structures, Smart Mater. Struct. 24 (2015) 045011, https://doi.org/10.1088/0964-1726/24/4/045011.
[53] M. Saafi, L. Tang, J. Fung, M. Rahman, F. Sillars, J. Liggat, X. Zhou, Graphene/fly ash geopolymeric composites as self-sensing structural materials, Smart Mater. Struct. 23 (2014) 065006, https://doi.org/10.1088/0964-1726/23/6/065006.
[54] C. Liu, G. Liu, Z. Ge, Y. Guan, Z. Cui, J. Zhou, Mechanical and self-sensing properties of multiwalled carbon nanotube-reinforced ECCs, Adv. Mater. Sci. Eng. 2019 (2019).
[55] S. Bi, M. Liu, J. Shen, X.M. Hu, L. Zhang, Ultrahigh self-sensing performance of geopolymer nanocomposites via unique interface engineering, ACS Appl. Mater. Interfaces 9 (2017) 12851–12858, https://doi.org/10.1021/acsami.7b00419.